International Journal of Multiphase Flow 142 (2021) 103700

Contents lists available at ScienceDirect

International Journal of Multiphase Flow

journal homepage: www.elsevier.com/locate/ijmulflow

Kelvin-Helmholtz instability governs the cavitation cloud shedding in Venturi microchannel

Darjan Podbevšek[a], Martin Petkovšek[a], Claus Dieter Ohl[b], Matevž Dular[a,b,*]

[a] Faculty of Mechanical Engineering, University of Ljubljana, Askerceva 6, 1000 Ljubljana, SI-Slovenia
[b] Institute for Physics, Otto von Guerricke University, Universitätsplatz 2, 39106 Magdeburg, DE-Germany

ARTICLE INFO

Article history:
Received 21 October 2020
Revised 26 February 2021
Accepted 23 May 2021
Available online 26 May 2021

Keywords:
Cavitation
Kelvin-Helmholtz instability
Venturi Microchannel

ABSTRACT

The paper shows visualization of cavitation inside a micro-Venturi channel. While the initial aim of the study was to establish supercavitating conditions inside a micro-Venturi, yet we found that this regime is suppressed due to the formation of a Kelvin-Helmholtz instability, which triggers a semi periodical attached cavity collapse. In depth observations using high speed imaging with visible light and X-rays revealed that this is, besides the re-entrant jet and the shock wave, a third mechanism leading to the shedding of cloud cavitation. In addition, a simple model was proposed which explains the formation of the Kelvin-Helmholtz instability in cavitating micro-Venturi and also offers explanation on why this is the dominant mechanism of cavitation cloud shedding at small scales.

© 2021 The Author(s). Published by Elsevier Ltd.
This is an open access article under the CC BY license (http://creativecommons.org/licenses/by/4.0/)

1. Introduction

Cavitation, characterized as inception, growth, and collapse of small vapour-gas bubbles is a physical phenomenon caused by a local change in the pressure. In hydraulic machinery it is often an undesirable and, in many cases, unavoidable, phenomenon. It causes vibration, noise, deterioration of efficiency, and even erosion of the elements of the flow tract.

It is known that cavitation behavior and its dynamics may change when scaling down the flow tract (Medrano et al., 2011; Mishra and Peles, 2005). At larger scales (order of centimeters) one of the most distinctive characteristics of developed cavitation is the process of cavitation cloud shedding. Detailed studies by Dular et al. (2005b, 2007), Ganesh et al. (2016, 2017) and Laberteaux and Ceccio (2001a, 2001b) helped to reveal two mechanisms that govern the shedding process:

- Re-entrant jet: due to the differences in the pressure inside and outside of the attached cavity, the flow, which passes it, deviates towards the surface of the submerged object A stagnation point forms just downstream of the attached cavity closure line and separates the flow into upstream and downstream parts. The former enters the attached cavity, and upon losing the momentum, causes its separation - forming a detached cavitation cloud. It is then carried downstream, where it enters a higher-pressure region and collapses. The process then repeats periodically.
- Shock wave: the collapse of the cavitation cloud causes a shock wave that spreads through the flow field. As it travels upstream, it suppresses the attached cavity. When the discontinuity in void fraction reaches the region of cavity attachment at the wedge apex, a large vapour cloud is shed. Later on, the cavity grows again and the process repeats.

With decreasing the size, the viscous forces start to become relevant as the Reynolds number drops. It was shown for example by Dular et al. (2012) that at a scale of several millimeters and below the re-entrant jet cannot fully develop – mainly due to a relatively larger bubbles compared to the size of the flow tract. As a result, the cavitation cloud shedding process ceases its periodic behavior and becomes chaotic.

Microfluidics is an exciting filed of research as it offers the possibility of using minute quantities of precious or toxic fluids, allowing us to study different fundamental phenomena in fluid dynamics (Ayela et al., 2013; Kim et al., 2017; Podbevsek et al., 2018; Stieger et al., 2017). However, by reducing the size of the channels to a sumbilimeter scale new properties of the flow are revealed. As the Reynolds number drops, the viscous and surface tension forces start to affect the dynamics of the vapor bubbles, what results in effect such as increased discrepancies in inception and desinent cavitation numbers due to lack of cavitation nuclei – liquid metastability (Medrano et al., 2012; Mishra and Peles, 2005). These are mostly consequences from the reduction of free stream

* Corresponding author.
E-mail address: matevz.dular@fs.uni-lj.si (M. Dular).

https://doi.org/10.1016/j.ijmultiphaseflow.2021.103700
0301-9322/© 2021 The Author(s). Published by Elsevier Ltd. This is an open access article under the CC BY license (http://creativecommons.org/licenses/by/4.0/)

nuclei and a lack of nucleation on channel walls (Medrano et al., 2011).

There are some mentions that Kelvin-Helmholz instabilities could exist in cavitating flow. Franc (2006) mentions its appearance in a single phase flow downstream of the separation point and discusses its cntribution to the cavitation inception. Aeschlimann et al. (2012) observed it in cavitating shear layer. Shao et al. (2018) performed measurements on a supercavitating bluff body and observed Kelvin-Helmholtz instability near its closure. Kong et al. (1999) discuss cavitation in diesel injector nozzle where they mention the occurrence of Kelvin-Helmholtz instability and its importance on the jet breakup. Similarly, Tonini (2006) relates it to the mechanism of jet atomisation. Finally, Brandner et al. (2010) observed it at high cavitation numbers inside the separating laminar shear layer and relates it to cavity breakdown.

Looking at the past works, the scientific community is well aware of the Kelvin-Helmholtz instability presence in cavitating flow, yet only few associate it with the global behaviour of the cavitation cloud shedding process. Till now no detailed study has been performed in terms of investigating Kelvin-Helmholtz instability as one of possible governing cavitation shedding mechanisms at fully developed cavitating flow.

Understanding the cavitation dynamics on a submillimeter scale is of a crucial importance for applications in the automotive industry. In fuel injection systems, the fuel is sprayed into the cylinder through a nozzle with a diameter of much smaller than a millimeter. While cavitation is always present, on one hand its appearance is desirable, as is promotes atomization of the fuel, leading to more efficient combustion, but on the other hand it causes erosion to the nozzle. An in-depth understanding of cavitation dynamics on these small scales is therefore essential for optimization. The second application is water treatment, where cavitation and its effects are used to destruct bacteria or inactivate viruses. For such application it is sometimes essential to establish supercavitating conditions in relatively compact channels (Šarc et al., 2018). Thus, an understanding of small-scale instabilities in such geometries is of crucial importance.

2. Experimental set-up

Experiments were performed at University of Ljubljana (Slovenia), Otto von Guericke University Magdeburg (Germany) and at Argonne National Laboratory – Advance photon source (USA). In all locations the same experimental setup was used.

2.1. Venturi section and the test rig

The experimental set-up is shown in Fig. 1. Venturi microchannels are made of 450μm thick stainless-steel sheets that include a laser cut convergent-divergent constriction by sandwiching them between two acrylic glass plates of 10mm thickness, see Fig. 1 (right, test section side view). The convergent-divergent (18°–10°) constriction has a throat height of 675 μm. The wall thickness along the constriction (Fig. 1 – Observation area) has been thinned to 2 mm, to minimize the X-ray absorption in the acrylic and provide better phase contrast. Inlet and outlet holes are drilled into the back layer of the acrylic glass plate to allow for the connecting tubes to feed the liquid into and out of the channel. Holes around the cut-out geometry are fitted with bolts to seal and place the sandwich test section together. The four bottom holes are used to mount the test section.

A small gear pump (1) transports liquid from the reservoir (2) through the 10μm nylon and 1μm glass fiber filter (3). The back-pressure regulator (4) limits the flow on the primary line of the setup, therefore setting the upstream pressure in the micro-Venturi (5). A safety relief valve (6) is installed in the system to prevent over-pressurization in case of clogging or user error. The flow from the channel and the two valves is then gathered back to the reservoir.

Experiments were performed at various operating conditions. From all results the same conclusions could be made. In the paper we only show results obtained at upstream pressure of 6 bar and mass flow rate of 11.9 g/s. At these conditions the flow velocity in the throat was approximately 39 m/s, leading to Re number of Re=21000 and cavitation number σ=0.785.

2.2. High speed visualization

Images were captured by either CMOS high speed cameras (Photron SA-Z and Photron Mini AX200) at a framerate of typically 200,000 fps. At this rate the image resolution was 384 × 176 pixels (25 μm/pixel for an integral view and 8 μm/pixel for a detailed view).

A modellocked fiber-based femtosecond laser (EXPLA FemtoLux 3, 515 nm wavelength) was used for backlite illumination. Approximately 200 fs long laser pulses were synchronized with the image acquisition such that a single laser pulse illuminated each frame. This technique allowed us to avoid all motion blurring and imaging of the shock waves if present.

2.3. Synchrotron measurements

High speed X-ray visualization was performed at the Argonne National Laboratory – Advance photon source. A Photron SA-Z high-speed camera recorded the image projected onto a scintillator screen with a 7.5× magnification, allowing us to capture a 1.3 × 1.3 mm image, which is roughly the size of the X-ray beam. We used every fourth pulse from the beam, which led to a frame rate of

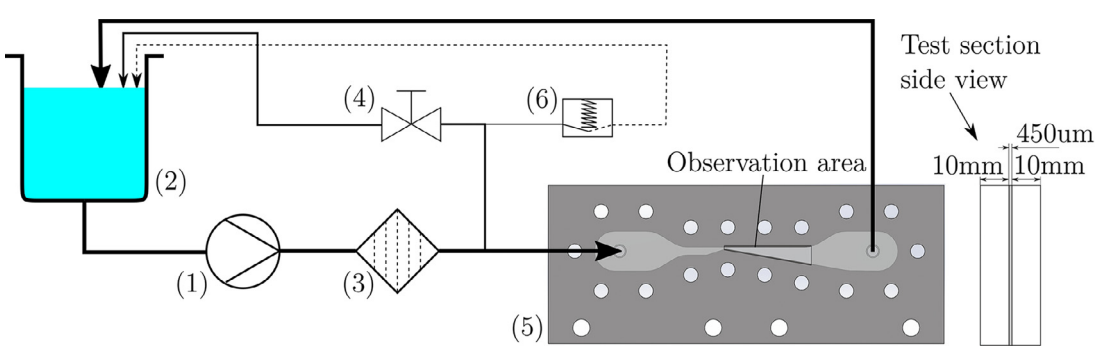

Fig. 1. Schematic presentation of the experimental set-up, with individual elements: gear pump (1), reservoir (2), filter (3), back pressure regulator (4), test section (micro-Venturi) (5), safety valve (6).

67,888 fps. The X-ray beam energy was adjusted with the undulator gap, between 7 to 40 keV.

The phase contrast imaging technique, explained in detail in (Khlifa et al., 2017), allows for imaging throughout the depth of the channel, revealing details that would be unseen or likely misinterpreted in classical backlight high-speed imaging. The bubble interphase that is parallel to the incoming beam attenuates the light creating regions of low and high intensity on the projected scintillator screen, which then converts the X-ray to visible light that is recorded by the high speed camera.

3. Results

3.1. General observations

Fig. 2 shows typical images of the Kelvin-Helmholtz instability occurrence in two different micro-Venturi channels. The flow is from the left tot the right.

The selected images do not belong to the same sequence and are shown only as a representation of the cavitation structure topology in the channel. We can obviously observe the rise of the interface and the subsequent roll-up of the waves, that eventually leads to the gradual collapse of the attached cavitation structure. The size of the channel does not play a significant role in the process as long it is small enough. At large dimension the attached cavity will consist of a number of small cavitation bubbles (cloud of bubbles), but when the throat of the channel is small enough (compared to the size of cavitation bubbles) a single attached cavity will form (its topology is discussed in more detail later on), and this is the needed condition for the onset of the instability. The relative size and probability of occurrence of the instability grows as the channel size is reduced. In the following we show data only for the case of a larger channel (675 $\times$ 450 μm), since all the reasoning applies to both scales.

Fig. 3 provides an overview of the important flow features, which were observed in the Venturi microchannel.

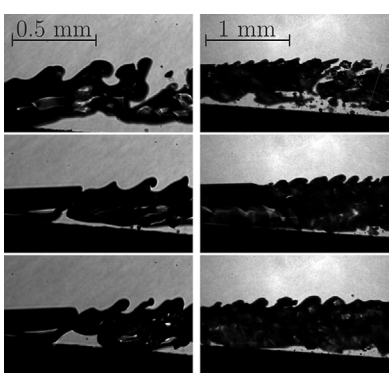

Fig. 2. Examples of Kelvin-Helmholtz instability occurrence in two different Venturi microchannels (left column: throat cross-section 225 $\times$ 450 μm, right column throat cross-section 675 $\times$ 450 μm; both Venturis have a 18° convergent and 10° divergent angles).

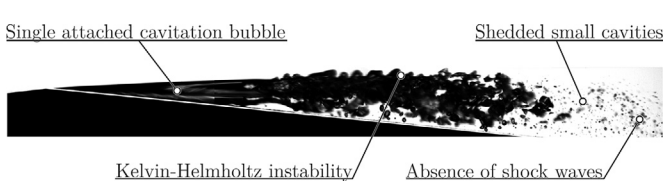

Fig. 3. General observations of the phenomena, which are unique for developed cavitation in Venturi microchannels. We observe single attached cavitation bubble, which is destabilised by the Kelvin-Helmholtz instability. The shedded cavities are very small and do not collapse violently enough to cause detectable shock wave emission.

Similar to our previous study of cavitation in milichannels (Dular et al., 2012) we find that cavitation in one respect resembles the condition of supercavitation – we see a single stretched cavitation bubble with a clear vapour-liquid interface. But in contrast to its macroscopic manifestation the one in the micro-Venturi is not stable. Its size oscillates periodically to large extent and small cavitation structures are shed from its closure. A second difference to the larger scales (Petkovšek et al., 2020) is that no shock waves are observed, that should be clearly visible with the femtosecond pulsed laser illumination. Instead at interface between the quasi supercavitating bubble and the liquid jet is wavy and oscillating. We identify this shape as a result of the Kelvin Helmholz instability. It will be shown later that this instability is not only causing the oscillation of the attached cavity but also results in the shedding of cavitation clouds.

Overall, four phenomena, which are generally not evident in developed cavitating flow in channels with larger dimensions, could be determined. Namely i) formation of a single attached cavitation bubble, ii) no shedding of larger cavities, iii) formation of Kelvin-Helmholtz instability and iv) the absence of shock waves from shedded cavity collapse. In the following sections each observation in more thoroughly discussed.

3.1.1. Single attached cavitation bubble

In our previous investigation of cavitation in milli-channel (Dular et al., 2012) we found that reducing the effective diameter of the channel from d_{nom} = 10 mm to d_{nom} = 3 mm considerably alters the structure of the cavity. In larger channels the attached cavity is always composed of numerous cavitation bubbles, while in the smaller channels, the vapor structure consists of finite number of large (compared to the section size) individual bubbles. This was later again shown by fast X-ray imaging (Coutier-Delgosha et al., 2009; Khlifa et al., 2017). The flow that we observe in the present micro-Venturi channel supports (and “extrapolates”) the findings in the milli-scale channels. A large (compared to the section size) single cavitation bubble stretches from the inception point downstream until the pressure increases well above the saturation pressure. With its clear single bubble interface, the topology as such resembles supercavitation found in macroscopic flows, but in contrast to macroscopic flow, it is only short lived here, due to the onset of the Kelvin-Helmholtz instability, which destabilizes it. Therefore, we could call this regime unstable quasi-supercavitation.

3.1.2. Kelvin-Helmholz instability

The attached single cavitation bubble stretches from the inception point and grows up to its largest extent, where a stagnation point forms near its closure. As the bubble ceases to grow, a shear flow between the bubble interface and the liquid jet above forms. This discontinuity in the velocity induces vorticity at the interface, which becomes unstable, grows and eventually rolls up into a spiral. The roll-up causes separation of small cavities and pushes the stagnation point further upstream. The process is continuous and ceases at the moment the inertial and surface tension forces overcome the instability. This is the case when the local static pressure is low enough for the cavity to grow at a velocity close to the velocity of the liquid jet, thus minimizing the shear between the phases.

Although Kelvin-Helmholtz instabilities are likely to occur in larger scale flows, too, yet their “strength” and importance for the general dynamics is marginal at fully developed cavitating flow. In larger channels instead the re-entrant jets and shock wave induced cavitation cloud shedding are dominant. This is due to the fact that the time constant of the Kelvin Helmholtz instability is longer and its effect may also be diminished by the 3D flow conditions, which is not the case inside the Venturi microchannel.

3.1.3. Small shedded cavities

In macro channel developed cavitating flow is characterized by shedding of large vaporous structures (clouds of bubbles), although recently, observations of secondary small-scale cavities were also reported by Arabnejad et al. (2019 Gnanaskandan and Mahesh (2016). The frequency of shedding is overall governed by the Strouhal number, which typically lies in the range between 0.1 and 0.5 (Dular and Bachert, 2009):

$$Str = \frac{f \cdot L}{v} = 0.1 \ldots 0.5. \quad (1)$$

It is important to note that a precise definition of the variables for the Strouhal number is somewhat arbitrary. Hence the Strouhal number law (Eq. (1)) as such, can lead to misleading interpretations (Dular and Bachert, 2009). Usually, v refers to the free stream velocity, L to the length of the attached cavity, just before the cloud separation, while f is the cloud shedding frequency.

In milli-channel it is observed that the confinement of the cavity, together with the growing ratio between the bubble size and the throat size, contribute to an inability of the reverse flow to cut the cavity and provoke its partial detachment (Dular et al., 2012). This leads to a more or less pronounced low-frequency oscillations of the attached cavity in absence of shedding. The value of the Strouhal number therefore reduces significantly. The shedding inside the present Venturi microchannel is governed by the Kelvin Helmholtz instability. Small cavitation structures are continuously shed from the cavity closure line which is rolled up as a result of the fully developed Kelvin Helmholtz instability. The dynamics of small cavity shedding appears similar to the one reported by Arabnejad et al. (2019) in larger channels, but there it is a result of either re-entrant jet or detachment due to rollup and not due to the Kelvin-Helmholtz instability.

This process is interrupted from the moment the attached cavitation bubble reaches its smallest size to the instant the largest size is reached and the onset of the rollup due to the Kelvin-Helmholtz instability shortly later. Continuous shedding is then repeated and lasts approximately one order of magnitude longer than the no-shedding period.

3.1.4. Absence of shock waves

Numerous studies report emissions of shock waves at cavitation cloud collapses (for example (Petkovšek et al., 2020)). These are related to a number of unwanted effects of cavitating flow – erosion, noise, vibration. In the present configuration we could not observe any shockwaves, despite the used technique was the same, and even improved one, that has been used previously in macroscopic channels. A possible explanation for that may be, that the collapse of the small shedded cavitation bubbles is significantly slowed down by the presence of the nearby channel walls – an effect which would not take place in a larger channel. Such weakened collapse pressure waves would be difficult to detect with the current pulsed laser setup.

3.2. The dynamics of cavitation cloud shedding

Particularly interesting is the onset of the Kelvin-Helmholtz instability and its contribution to the dynamics of cavitation structure shedding process. Fig. 4 shows a typical cycle of the attached cavity oscillation.

From the observation of the entire flow field (Fig. 4) it is obvious that the process of destabilization of the attached cavitation pocket is initiated at the cavity closure line. The attached cavity firstly grows to the size shown in frame (1), where one can see the fully extended attached cavitation bubble. Due to the divergent angle of the Venturi the flow velocity decreases, and the pressure increases to a value at which further growth is limited. At the cavity closure line the re-entrant jet builds up (frame 2). As the growth of the cavity stagnates, significant shear flow forms between the vapour and the liquid at the interface. The rear part of the cavity begins to oscillate mildly that affects the pressure balance. A decreased gap between the interface and the upper channel wall forces the liquid jet to accelerate, what induces a local drop in the pressure above the interface. A newly established pressure difference pushes the interface further and the disturbance grows. At the same time the shear flow stretches the interface and by this builds a vortex - the Kevin-Helmholtz instability forms. As the interface curls up, it becomes unstable and eventually breaks up, shedding multiple small vaporous cavities (possibly single bubbles) downstream (frames 3 to 5). The new cavity closure line moves upstream and the process is continued until a low-pressure region, closer to the throat of the Venturi is reached (frame 6). At this point the cavitation pocket is somewhat stabilized and begins to grow at a slightly slower pace than the velocity of the liquid jet. As a result, the shear flow, although smaller, is still present - cavity shedding due to the presence of the Kelvin-Helmholtz instability continues (frames 7 to 11). The cavity growth accelerates and reaches the same velocity as the liquid jet. Hence, the shear flow is minimized, the cavity interface becomes stable, and the shedding briefly ceases before the cycle is repeated.

A more detailed look into the unstable interface can be obtained from the high speed recording using the X-Ray imaging. This phase-contrast enhancement technique provided by the APS (Advanced Photon Source) synchrotron beam is presented in Fig. 5.

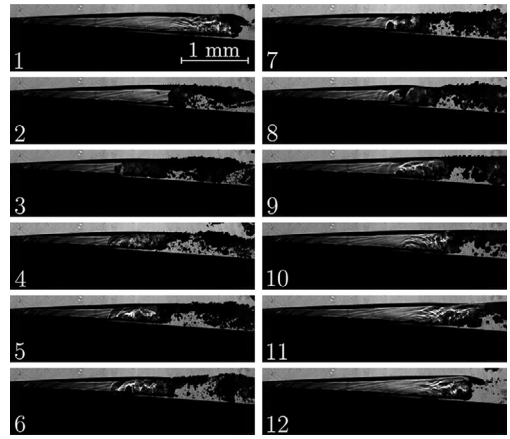

Fig. 4. A sequence showing one cycle of a typical shedding period in a 675 × 450 μm Venturi channel. The time difference between two images is 0.1ms. In images No. 2, 3, 8, 9 and 10 one can observe the occurrence of Kelvin-Helmholtz instability.

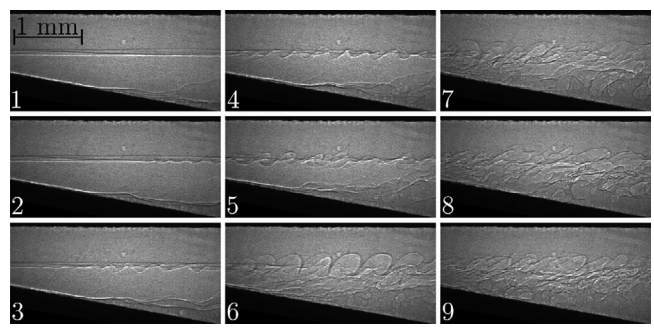

Fig. 5. A sequence taken during an experimental campaign by fast x-ray imaging in a 675 × 450 μm Venturi channel. The time difference between two images is 0.1 ms. One can clearly observe the occurrence of Kelvin-Helmholtz instability from frame 2 to 7, with the following frames showing the breakup of the attached single cavitation bubble.

It allows us to observe the hidden features of the vaporous cavity, as it starts developing surface instabilities and leads to its breakup.

The first frame of Fig. 5 depicts a smooth interface between the liquid jet and the vapour phase. Close to the channel wall (frame 1 and 2) one can see a thin liquid layer which slowly moves upstream. This is a result of a separation of the cavitating structure from the wall and the very weak classical re-entrant jet. The stagnation of the cavity growth results again in a shear flow at the interface and the Kelvin-Helmholtz instability builds up, firstly at the cavity closure before it moves upstream (frames 2 to 4). At the same time, the attached cavity is still in a form of a stretched single bubble. In frame 5 one can observe the beginning of the rollup, which becomes more pronounced in frame 6. Finally, as a result of Kelvin-Helmholtz instability, we witness the breakup of the attached cavity in frames 7 to 9.

The phenomenon likely also occurs in larger geometries, but does not develop fully, due to very small changes in shear velocities at the interface. This is further discussed in the following section.

4. Discussion

A very simple model, based on Bernoulli's equation is sketched in Fig. 6 to explain the dynamics in the channel.

The flow in the channel is bounded by two walls. The channel width is given by w. The position of the initial interface (black dotted line) lies between the upper and the lower channel wall and let us assume that it already exhibits a small initial disturbance – its height ψ is not constant over the length of the channel. The velocities on each side of the interface (u_1 and u_2) are determined by the flow rate and by the local position of the interface $\psi(x,t)$. The static pressures (p_1 and p_2) are considered constant and homogeneous in the liquid and vapour phase.

We now derive an expression for the displacement of the interface in the vertical ($\Delta\psi$) and horizontal ($\Delta\delta$) direction. Eventually this results in the formation of the Kelvin-Helmholtz instability indicated with a gray dotted line in Fig. 6.

Let us approach the displacement of a fluid element in the vapor phase with length Δx, height ψ and width w. There, four forces are acting, namely gravity F_g, surface tension F_σ, viscous drag F_μ, on one side and the pressure difference $F_{\Delta p}$ on the other. Using Newton's 2nd law, one can write for the vertical acceleration a_y:

$$m \cdot a_y = \rho_v \cdot \Delta x \cdot \psi \cdot w \cdot a_y = \sum^F = F_g + F_\sigma + F_\mu + F_{\Delta p}, \tag{2}$$

where ρ_v is the vapour density, ψ is the height of the interface above the bottom wall. The gravitational force is of course given by the weight of the element:

$$F_g = -\ m \cdot g = -\ \rho_v \cdot \Delta x \cdot w \cdot \psi \cdot g, \tag{3}$$

with g being the gravitational acceleration, pointing downwards. The surface tension force is given by:

$$F_\sigma = \ -2 \cdot \Delta x \cdot \sigma, \tag{4}$$

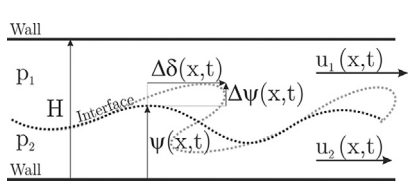

Fig. 6. Schematic presentation of the interfacial instability, with variables which define the problem.

Table 1
Parameters of the calculations.

	Micro	Mili	Macro
H	0.675 mm	2.7 mm	10 mm
w	0.45 mm	3.6 mm	10 mm
$\mathbf{v_{throat}}$	39 m/s	17 m/s	24.7 m/s
L	5·H		
λ	L/10		
A	1 μm		
$\boldsymbol{\mu}$	0.001 Pas		
$\boldsymbol{\rho_l}$	1000 kg/m^3		
$\boldsymbol{\rho_v}$	1 kg/m^3		

where σ is the surface tension coefficient. The viscous drag, which attenuates the rise of the interface, is given by:

$$F_\mu = -\mu \cdot A \cdot \frac{v_y}{w} = -\mu \cdot \Delta x \cdot v_y, \tag{5}$$

where μ is the viscosity of the fluid. The three mentioned forces F_g, F_σ, F_μ, all act against the rise of the interface, with only the latter one having a significant contribution.

The pressure difference that drives the formation of instability results from the difference of the velocities on each side of the interface. The flow rate through the channel is assumed to be constant and uniform over the whole height of the channel, provided that the interface splits the channels into equal parts (H=2ψ, $u_{1,0} = u_{2,0}$). Hence the velocities on each side of the interface are solely a function of the interface position and change relatively with its displacement:

$$\frac{u_2}{u_1} = \frac{(H-\psi)}{\psi}. \tag{6}$$

The pressure difference and the corresponding driving force is then:

$$F_{\Delta p} = \left[\left(p_1 - \frac{1}{2}\rho_1 u_1^2\right) - \left(p_2 - \frac{1}{2}\rho_2 u_2^2\right)\right] \cdot \Delta x \cdot w. \tag{7}$$

Using a simple Euler scheme, the displacement of the interface $\Delta\psi$ during one time step Δt, can be written as:

$$a_y = \frac{\sum^F}{m} = \frac{\sum^F}{\rho_v \cdot \Delta x \cdot \psi \cdot w}, \tag{8}$$

$$\Delta v_y = a_y \cdot \Delta t, \tag{9}$$

$$\Delta\psi = v_y \cdot \Delta t. \tag{10}$$

The vortex builds due to the convection of the interface by the shear flow. It can be simply assumed that:

$$\Delta\delta = (u_1 - u_2) \cdot \ \Delta t. \tag{11}$$

In the presented calculation an initial disturbance ψ_0 in form of a constantly growing sinusoidal profile is given to the interface:

$$\psi_0 = A \cdot \sin\left(\frac{x}{\lambda}\right) \cdot \frac{x}{L}, \tag{12}$$

where A is the maximal amplitude and L is the length of the interface and λ is the wavelength of the disturbance.

Results of exemplary calculations are shown in Fig. 7. The geometries were chosen to correspond to the existing experiments – micro (present geometry), mili (Dular et al. (2012)) and macro (Petkovšek & Dular, 2013). Parameters for the calculations are given in Table 1. The values were chosen based on the parameters of the fluids and on geometry of the Venturi section. We have scaled the length of the cavity linearly (5·H, which results in the same size order as in the experiments) and assumed that the wavelength of the disturbance is always 1/10th of the cavity length. The initial

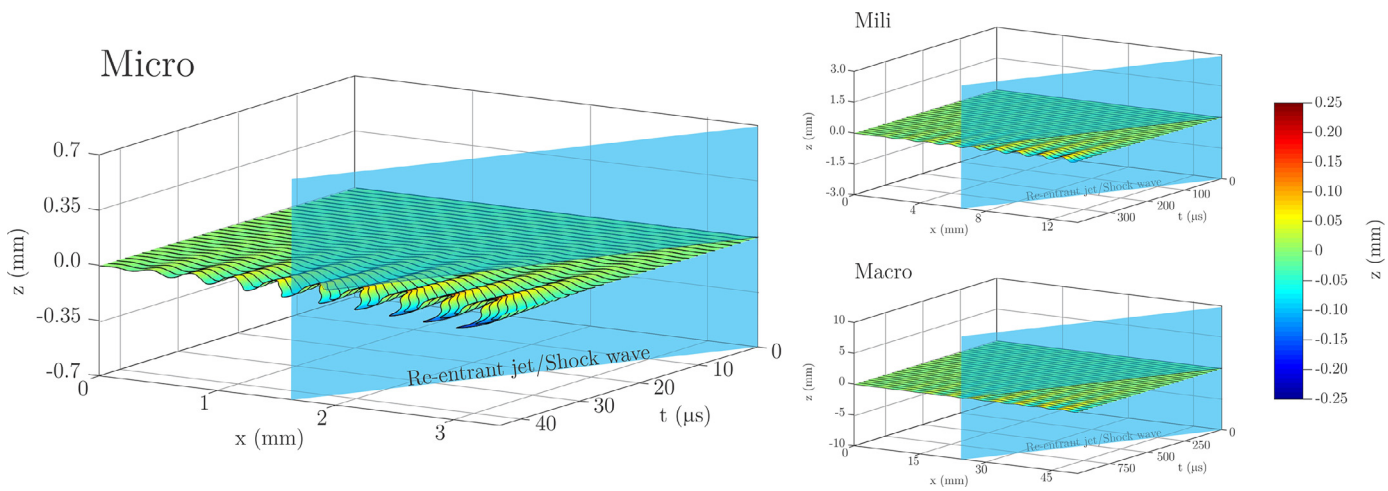

Fig. 7. Model prediction for micro (left), mili (right, top) and macro (right, bottom) Venturi channels.

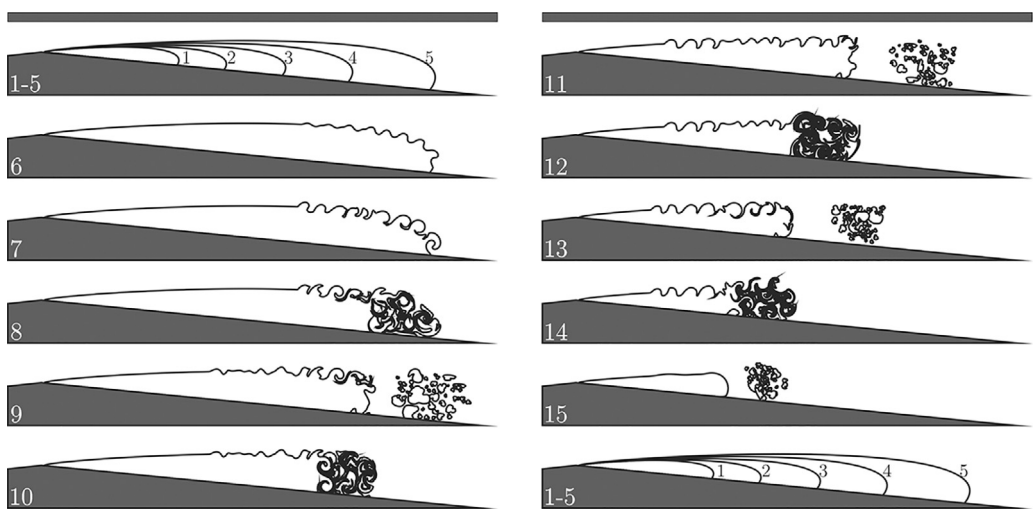

Fig. 8. Schematic representation of cavitation dynamics inside Venturi microchannel, which is governed mainly by the appearance of the Kelvin-Helmholtz instability.

disturbance is always 1mm, regardless of the size of the geometry. The velocities in the throat of the section correspond to the measured ones. The simulation begins at the time when the cavity reaches the maximum size and the stagnation point is established (t=0). At this moment the re-entrant jet would form and begin to flow upstream with a velocity in the order of v_{throat}. The prediction of the re-entrant jet is based on the assumption that it will travel upstream from the cavity closure line with a constant velocity, which is the same one as in the throat of the channel (Dular et al., 2005a). According to the results reported by Ganesh et al. (2016) the shock wave velocity would lie in the same order of magnitude. We cut off the calculation at the moment when the re-entrant jet/shock wave would penetrate 50% of the cavity length ($t=0.5L/v_{throat}$), upon which the cloud separation would likely occur.

The diagrams show the development of the instability in space and time. The blueish plane presents the estimated progression of the re-entrant jet/shoch wave.

For the microchannel (Fig. 7, left), one can see that the instability builds up rapidly and begins to bend over. At the point when the calculation is stopped (at 42 μs) the rear part of the cavity collapses (completely rolls up). Further on the waves near the cavity closure collide with the channel walls and the calculation diverges. One can assume that the disturbance would grow towards the cavity attachment point. When it would reach it could be be considered as the beginning of a growth of a new cavitation bubble.

The instability is already fully developed when the re-entrant jet penetrates 50% of the cavity. The height of the waves corresponds to roughly one half of the throat height - roughly the span observed experimentally, with X-ray imaging, shown in Fig. 5 (frame 6). This results in a significant disturbance of the flow, which would cause shedding of small vaporous bubbles, hence a classical vapour cloud separation does not occur. The Kelvin-Helmholtz instability can therefore be considered as the dominant mechanism of cavitation shedding process inside micro scale channel.

For the mili and macro channels (Fig. 7, right, top and bottom) the dynamics is similar. The instability is present, but it grows much slower. By the time the re-entrant jet would penetrate 50% into the cavity, the disturbance is still very small compared to the channel height (5% for mili and 1.5% for macro channel). Also, no evidence of rollup, which finally causes the collapse of the whole cavity, can be seen.

Considering the insignificance of the Kelvin-Helmholtz instability, one can confidently claim that the re-entrant jet or the shock wave are the dominant mechanisms of cloud shedding in larger geometries, even if one assumes perfectly 2-dimensional flow conditions in such channels.

Fig. 8 sums up our observations - a schematic representation of the dynamics of cavitation inside a very small Venturi channel is shown. It shows how the cavity grows, the appearance of the Kelvin-Helmholtz instability, the collapse of the sta-

ble cavity and finally the consequent growth of the new attached cavity.

The shedding period begins with the growth of an attached single cavitation bubble (1–5). During this period the bubble growth rate follows the velocity of the liquid flow above it, hence the shear at its interface in minimal. At (5) the cavity ceases to grow, and a stagnation point is formed at its closure. The flow of a liquid jet that travels over the momentarily stable cavitation bubble causes velocity and pressure discontinuity over the bubble interface. The pressure difference promotes the growth of small disturbances (6). The disturbances grow and at the same time begin to rollup (7) and eventually collapse (8). Small remaining cavitation structures are advected downstream (9). The process is continuous and works its way upstream (10–15). At (15) the remaining single bubble cavity is small enough for the surface tension to stop the shedding at which point the process is periodically repeated (1–5).

5. Conclusions

There are some mentions that Kelvin-Helmholz instabilities could exist in cavitating flow in microchannels, but this has not been investigated thoroughly. Here we show detailed observations of Kelvin-Helmholtz instability, and demonstrate that its occurrence destabilizes single cavitation bubble structure in Venturi microchannels. This is due to the uniquely confined flow, which triggers the Kelvin- Helmholtz instability from the cavity closure line. The flows were investigated by high speed image capturing with femtosecond laser pulses light and X-rays. The recordings reveal how the instability forms, grows and eventually triggers the shedding of relatively small cavities. The second result of the study is lack of shock waves, typically observed upon the collapse of the shedded bubbles downstream. Finally, we developed a simple model, based on the force balance of fluid particle in the vapor phase and the Bernoulli equation. By comparison of the calculations for small and large channels, we show that only in the small channels, the Kelvin-Helmholtz instability drives the cavitation cloud shedding process, while in larger channels the shedding is driven either by the re-entrant jet or by the shock wave mechanisms.

Declaration of Competing Interest

The authors declare that they have no known competing financial interests or personal relationships that could have appeared to influence the work reported in this paper.

CRediT authorship contribution statement

Darjan Podbevšek: Investigation, Writing – original draft. **Martin Petkovšek:** Investigation, Writing – original draft, Writing – review & editing. **Claus Dieter Ohl:** Methodology, Writing – original draft. **Matevž Dular:** Conceptualization, Visualization, Writing – original draft, Writing – review & editing, Supervision.

Acknowledgments

The authors acknowledge the financial support from the European Research Council (ERC) under the European Union's Framework Program for research and innovation, Horizon 2020 (grant agreement n 771567 – CABUM) and the Slovenian Research Agency (Core funding No. P2-0401 and project No. J7-1814). This research used resources of the Advanced Photon Source, a U.S. Department of Energy (DOE) Office of Science User Facility operated for the DOE Office of Science by Argonne National Laboratory under Contract No. DE-AC02-06CH11357. Finally, M. Dular acknowledges the support from the Humboldt Foundation Friedrich Wilhelm Bessel Research Award.

References

Aeschlimann, V., Prothin, S., Barre, S., Djeridi, H., 2012. High speed visualizations of the cavitating vortices of 2D mixing layer. Eur. J. Mech. B/Fluids 31 (1), 171–180.
Arabnejad, M.H., Amini, A., Farhat, M., Bensow, R.E., 2019. Numerical and experimental investigation of shedding mechanisms from leading-edge cavitation. Int. J. Multiphase Flow 119, 123–143.
Ayela, F., Medrano-Muñoz, M., Amans, D., … Ledoux, G., 2013. Experimental evidence of temperature gradients in cavitating microflows seeded with thermosensitive nanoprobes. *Phys. Rev. E* 88 (4) 043016-(1-5).
Brandner, P.A., Walker, G.J., Niekamp, P.N., Anderson, B., 2010. An experimental investigation of cloud cavitation about a sphere. J. Fluid Mech. 656, 147–176.
Coutier-Delgosha, O., Vabre, A., Hocevar, M., … Lee, W.K., 2009. Local measurements in cavitating flow by ultra fast X-ray imaging. In: Proceedings of the ASME Fluids Engineering Division Summer Conference 2009, FEDSM2009, 2. American Society of Mechanical Engineers Digital Collection, pp. 371–379.
Dular, M., Bachert, R., 2009. The issue of strouhal number definition in cavitating flow. J. Mech. Eng. 55 (11), 666–674.
Dular, M., Bachert, R., Schaad, C., Stoffel, B., 2007. Investigation of a re-entrant jet reflection at an inclined cavity closure line. Eur. J. Mech. B/Fluids 26, 688–705.
Dular, M., Bachert, R., Sirok, B., Stoffel, B., 2005a. Transient simulation, visualization and PIV-LIF measurements of the cavitation on different hydrofoil configurations. J. Mech. Eng. 51 (1), 13–27.
Dular, M., Bachert, R., Stoffel, B., Širok, B., 2005b. Experimental evaluation of numerical simulation of cavitating flow around hydrofoil. Eur. J. Mech. B/Fluids 24, 522–538.
Dular, M., Khlifa, I., Fuzier, S., Adama Maiga, M., Coutier-Delgosha, O., 2012. Scale effect on unsteady cloud cavitation. Exp. Fluids 53 (5), 1233–1250.
Franc, J.-P., 2006. *Physics and Control of Cavitation. Design and Analysis of High Speed Pumps*.
Ganesh, H., Mäkiharju, S.A., Ceccio, S.L., 2016. Bubbly shock propagation as a mechanism for sheet-to-cloud transition of partial cavities. J. Fluid Mech 802, 37–78.
Ganesh, H., Mäkiharju, S.A., Ceccio, S.L., 2017. Bubbly shock propagation as a mechanism of shedding in separated cavitating flows. J. Hydrodyn. Ser. B (English Ed.) 29 (6), 907–916.
Gnanaskandan, A., Mahesh, K., 2016. Large Eddy Simulation of the transition from sheet to cloud cavitation over a wedge. Int. J. Multiphase Flow 83, 86–102.
Khlifa, I., Vabre, A., Hočevar, M., … Coutier-Delgosha, O., 2017. Fast X-ray imaging of cavitating flows. *Exp. Fluids* 58 (11), 157.
Kim, J., Michelin, S., Hilbers, M., … Gacoin, T., 2017. Monitoring the orientation of rare-earth-doped nanorods for flow shear tomography. *Nat. Nanotechnol.* 12 (9), 914–919.
Kong, S.C., Senecal, P.K., Reitz, R.D., 1999. Developments in spray modeling in diesel and direct-injection gasoline engines. Oil Gas Sci. Technol. 54 (2), 197–204.
Laberteaux, K.R., Ceccio, S.L., 2001a. Partial cavity flows. Part 1. Cavities forming on models without spanwise variation. J. Fluid Mech. 431, 1–41.
Laberteaux, K.R., Ceccio, S.L., 2001b. Partial cavity flows. Part 2. Cavities forming on test objects with spanwise variation. J. Fluid Mech. 431, 43–63.
Medrano, M., Pellone, C., Zermatten, P.J., Ayela, F., 2012. Hydrodynamic cavitation in microsystems. II. Simulations and optical observations. Phys. Fluids 24 (4), 047101.
Medrano, M., Zermatten, P.J., Pellone, C., Franc, J., Ayela, F., 2011. Hydrodynamic cavitation in microsystems. I. Experiments with deionized water and nanofluids. Phys. Fluids 23 (12), 127103.
Mishra, C., Peles, Y., 2005. Cavitation in flow through a micro-orifice inside a silicon microchannel. Phys. Fluids doi:10.1063/1.1827602.
Petkovšek, M., Dular, M., 2013. Simultaneous observation of cavitation structures and cavitation erosion. Wear 300 (1-2), 55–64.
Petkovšek, M., Hočevar, M., Dular, M., 2020. Visualization and measurements of shock waves in cavitating flow. Exp. Therm. Fluid Sci. 119, 110215.
Podbevsek, D., Colombet, D., Ledoux, G., Ayela, F., 2018. Observation of chemiluminescence induced by hydrodynamic cavitation in microchannels. Ultrason. Sonochem. 43, 175–183.
Šarc, A., Kosel, J., Stopar, D., Oder, M., Dular, M., 2018. Removal of bacteria Legionella pneumophila, Escherichia coli, and Bacillus subtilis by (super) cavitationm Ultrasonics sonochemistry 42, 228–236.
Shao, S., Wu, Y., Haynes, J., Arndt, R.E.A., Hong, J, 2018. Investigation into the behaviors of ventilated supercavities in unsteady flow. Phys. Fluids 30 (5), 052102.
Stieger, T., Agha, H., Schoen, M., Mazza, M.G., Sengupta, A., 2017. Hydrodynamic cavitation in Stokes flow of anisotropic fluids. Nat. Commun. 8 (1), 15550.
Tonini, S., 2006. Fuel Spray Modelling in Direct-Injection Diesel and Gasoline Engines. City University London.